Topographic amplification from recorded earthquake data and numerical simulations

C. Cauzzi & D. Fäh
Swiss Seismological Service (SED-ETHZ), Zürich, Switzerland

V. Pessina
Istituto Nazionale di Geofisica e Vulcanologia (INGV), Milano, Italy

E. Faccioli & C. Smerzini
Department of Structural Engineering, Politecnico di Milano, Italy

SUMMARY:
With the aim of contributing to the refinement of the next generation of tools for seismic hazard analyses, we present here an attempt at including topographic amplification factors in GMPEs, thus broadening the traditional options for site effects. With a view to critically discuss and complement with new data the approach of Cauzzi et al. (2010) and Paolucci (2002), information from additional numerical models including crustal layering are taken into account. The indications obtained from the numerical simulations are cross-checked against and consolidated by analyses of the residuals of a selection of strong- and weak-motion observations on topographic reliefs in Italy and Switzerland (carefully selected via GIS) with respect to a set of largely used GMPEs.

Keywords: topography, GMPEs, building codes

1. INTRODUCTION

Amplification of seismic waves due to topographic irregularities has been often addressed as one of the possible causes of localised earthquake damage, as well as of the initiation of earthquake induced phenomena, like landslides, which represent one of the major causes of earthquake-related devastation (Paolucci, 2002). From an observational perspective, amplification phenomena due to topography are often difficult to segregate from the effects of structural layering and near-surface geology, unless refined tomography models are available. As amplification due to near-surface geology typically exceeds morphologic amplification, the latter is generally disregarded in seismic building codes, with the exception of the Eurocode 8 (CEN, 2004), where frequency-independent amplification factors not larger than 40% are prescribed, based on the height and the slope of simple 2D relief configurations. The uncertainties associated with the quantification of topographic amplification result into the Eurocode prescription for refined analyses for complex geometries. The Eurocode 8 approach was adopted in 2008 by the Italian Building Code (Norme Tecniche per le Costruzioni, 2008), where four classes of topographic amplification are explicitly defined, as listed in Table 1.1.

Table 1.1. Topographic amplification factors prescribed by Italian Building Code (Norme Tecniche per le Costruzioni, 2008).

Topographic class	Description	Amplification factor
T1	Flat surface; isolated slopes and cliffs with average slope angle $i < 15°$	1
T2	Slopes with $i > 15°$	1.2
T3	Ridges with crest width significantly less than the base width and $15° < i < 30°$	1.2
T4	Ridges with crest width significantly less than the base width and $i > 30°$	1.4

Properly assessing topographic amplification is of key importance in the European context where a broad range of exposure levels to earthquake hazard is encompassed (Faccioli et al., 2002) and many

small towns are located at the top of isolated steep cliffs. Moreover, such unfavourable conditions often come together with high vulnerability levels of the built environment and the susceptibility to slope sliding (Paolucci, cit.). While remarkable efforts are documented in the literature aimed at collecting, interpreting and modelling topographic amplification phenomena, the possibility of directly introducing these effects into ground motion prediction equations (GMPEs) has been only recently addressed within the context of two Italian research projects (funded by DPC, namely S2 and S4), that addressed a broad range of engineering seismology topics.

3D Spectral Elements (SEM) numerical simulations were used in S2 to derive a functional representation of topographic amplification factors (http://nuovoprogettoesse2.stru.polimi.it). Cauzzi et al. (2010) compared the Displacement Response Spectra *DRS*(T;5%) as computed from the waveforms generated from numerical models with irregular and flat surface morphology. In most cases, they found that the topographic amplification factor *f(T,H,S)* could be reasonably modelled by a linear combination of terms proportional to normalised elevation *H*, to a power of *H*, and to local slope *S* (in degrees):

$$f(T,H,S;5\%) = a_1 + a_2 H + a_3 H^{a_4} + a_5 S_{10-20} + a_6 S_{20-30} + a_7 S_{>30} \pm \sigma \tag{1.1}$$

where *H*, normalised elevation in the interval [0;1], is defined as:

$$H = \frac{z - z_{\min}}{z_{\max} - z_{\min}} = \frac{z - z_{\min}}{\delta_1}. \tag{1.2}$$

While Eqn. 1.1 provided an attempt at modelling the functional form of topographic amplification in GMPEs, Cauzzi et al. (cit.) examined the additional problem or relating the modelled amplification with the vibration period *T* of the hill or mountain at hand. Starting from the work of Paolucci (2002), who applied the Rayleigh's method for estimating the fundamental vibration periods of homogeneous 2D reliefs as $\hat{T}_{0-SH} = W/(0.7\beta)$ and $\hat{T}_{0-SV} = W/\beta$ (based on the width *W* of the mountain cross-section and the shear wave velocity β) Cauzzi et al. (cit.) provided alternative estimates by representing the topographic irregularity as an idealised uniform fixed-free shear-beam, with vibration periods (see e.g. Blevins, 1979):

$$T_i = \frac{4\Delta}{(2i-1)\beta K^{1/2}}, \qquad i = 1,2,3... \tag{1.3}$$

where *G* is the shear modulus, ρ the mass density of the beam material, Δ the span of the beam and *K* the shear coefficient that they assumed equal to 1. The key input to the approach of Cauzzi et al. (cit.) was the following set of geomorphological parameters: a) maximum and minimum elevation of the mountain: z_{max} and z_{min}; b) elevation of the station *z*; c) local slope *S*; d) longitudinal extension of the mountain *L*; d) width of the mountain *W*; e) the crest width W_C; f) average shear wave velocity β (known for numerical models and to be estimated for real cases). Additionally, they adopted the shape factor of the ellipse of same base area and longitudinal extension of the mountain as a proxy for 2D/3D behaviour, and an alternative definition of the height of the relief δ_2, computed dividing the total volume of the mountain by the base area.
Research in S4 focused on the records of the Italian strong motion database (ITACA, http://itaca.mi.ingv.it) with the aim of identifying stations affected by site effects that are not captured by standard seismic classification schemes (Massa et al., 2010; Bindi et al., 2011). In particular, Bindi et al. (cit.) considered four different site classifications (two of them based on geological/geophysical characteristics and two driven by data) and calibrated *ad hoc* ground motion prediction equations with the aim of using the "between-station error normalized to the standard deviation of the between-station error distribution" to identify stations characterised by large errors, attributable to site effects not accounted for by the classification schemes. The results showed – as expected - that large errors can affect the predictions when the site effects are not uniquely related to the reduction in seismic

impedance in the uppermost layers.
With the above background, and with the aim of contributing to the refinement of the next generation of tools for seismic hazard analyses, we present here a further attempt at defining how to include topographic amplification factors in GMPEs, thus broadening the traditional options for site effects. With a view to critically discussing and complementing with new data the approach of Cauzzi et al. (cit.), information from additional numerical models including crustal layering are taken into account. The indications obtained from the numerical simulations are cross-checked against and consolidated by analyses of the residuals of a selection of strong- and weak-motion observations on topographic reliefs in Italy and Switzerland (carefully selected via GIS) with respect to a set of largely used GMPEs.

2. TOPOGRAPHIC AMPLIFICATION FROM SYNTHETIC DATA

The aim of this section is to complement with additional results from numerical modelling the preliminary investigations of Cauzzi et al. (2010) who used 3D synthetic waveforms generated from SEM (Faccioli et al., 1997) numerical models in: a) the Sulmona (Central Italy) area and b) the l'Aquila (Central Italy) area. As in the former study, the analyses were performed with the code GeoELSE (http://geoelse.stru.polimi.it, Stupazzini et al., 2009) and the computational mesh was created with CUBIT (http://cubit.sandia.gov/index.html). The model is briefly described in Section 2.1, while interesting results are selectively presented in Section 2.2.

2.1. Description of the model

The Irpinia (Southern Italy) test site was chosen in this study as the candidate for the generation of synthetic scenarios due to i) the availability of well-constrained and validated fault model and a reliable crustal structure; ii) the presence of interesting topographic features and iii) the reasonable number of real earthquake recordings of the simulated event (1980 Nov. 23, M_W 6.9) at the stations of the Italian strong-motion network (RAN), basic for checking the soundness of the synthetic waveforms. As apparent from Fig. 2.1, the model extends over a volume of about 85 x 83 x 35 km^3 and is discretised using an unstructured mesh of hexahedra with characteristic element size ranging from ~ 300 m at the surface to ~ 1200 m at the bottom of the model. Surface seismic motion at 256 receiver locations were generated from a single normal fault (35 x 15 km), with 60° NNE dip, 315° strike and 90°rake (Ameri et al., 2011).

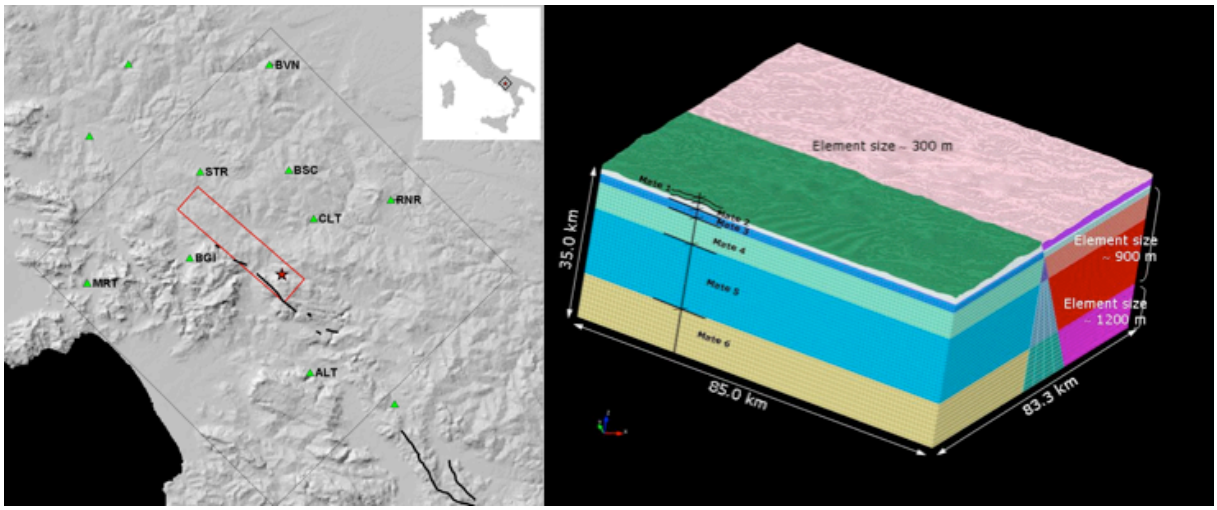

Figure 2.1. (rhs) Digital elevation model (DEM) of the 1980 Irpinia earthquake study area. The grey rectangle represents the boundaries of the numerical model. The red rectangle and the star are the surface projection of the ruptured fault and the epicentre location, respectively. Traces of the active faults in the area are depicted as black curves. Note the number of strong-motion stations in the study area (green triangles). (rhs) Numerical model, note the variable element size and the crustal layering adopted.

Two different scenarios were created assuming both a flat Earth surface and a realistic full 3D model with irregular topography, derived by a 250 m resolution digital elevation model (DEM). A 1D crustal structure was assumed (Tab. 2.1), adapted from Ameri et al. (2011), as well as a slip distribution model for the kinematic representation of the ruptured fault.

Table 2.1. 1D crustal model (modified after Cultrera et al., 2010)

Material number	Depth of layer, km	$V_S = V_P/1.81$, kms^{-1}	ρ, gcm^{-3}
1	1	1.2	2.2
2	2	1.93	2.3
3	4	2.49	2.5
4	10	3.15	2.6
5	25	3.59	2.7
6	35	4.14	2.9

2.2. Results

2.2.1. Topographic amplification at a glance

Fig. 2.2 shows the topographic amplification as computed at each monitored node (grey curves) on the surface of the numerical model. The mean and the standard error of the amplification values are also displayed as thick red curves. The amplification effect here is purely related to the irregular topography of the model, since the layering and the material properties are the same used for the flat model. The topographic amplification factor at each monitored node receiver *j* was computed as:

$$f_j(T;5\%) = \frac{DRS_{TOPO,j}(T;5\%)}{DRS_{FLAT,j}(T;5\%)} \tag{2.1}$$

where *DRS(T;5%)* is the 5%-damped elastic displacement response spectrum, as computed from the acceleration time histories obtained via double differentiation of the synthetic displacement histories, and the suffixes TOPO and FLAT refer to the waveforms generated with the irregular and the flat surface morphology, respectively. The horizontal components were combined through their geometric mean and the spectra were normalized (through multiplication by $R^{-a(T,5\%)}$, $a<0$) with respect to the hypocentral distance (R) using the coefficients for geometric attenuation (a) of the GMPE of Cauzzi and Faccioli (2008).

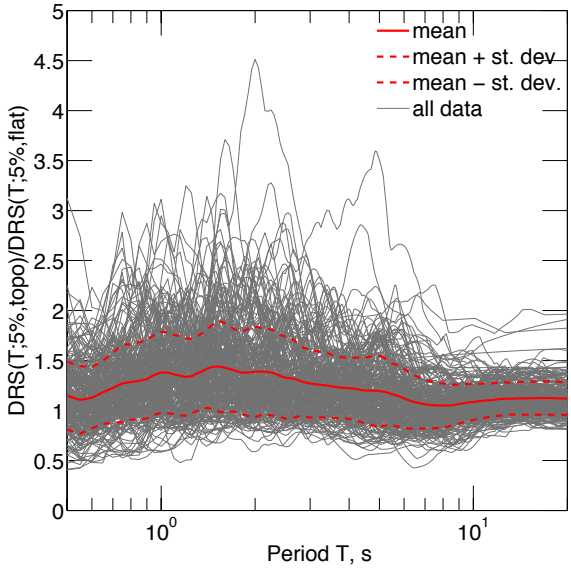

Figure 2.2. Summary plot of the topographic amplification factors as a function of period *T* obtained from numerical modelling of the Irpinia 1980 event, as described in the text.

As apparent from Fig. 2.2, large positive amplifications can be locally observed in the near-fault region of the model with irregular topography, up to a factor of 4.5. On the other hand, negative amplification (a factor of 2, at most) occurs as expected at a number of receivers, most likely located at the foot of topographic irregularities or in complex geometrical configurations. Amplification peaks tend to populate the period range between 0.5 s (the resolution limit of the model) and 10 s for the case at hand.

2.2.2. Amplification at complex 2D topographic irregularities

One of the most interesting and densely monitored topographic features in the model is represented by the mountain range of the Alburni (Fig. 2.3). This topographic irregularity extends for ~ 27 km in the longitudinal direction (L), with a representative width W 13.7 km in the transverse direction and would be classified therefore as a 2D structure. However, due to its relatively steep slopes and the flat topography of the crest in the NW part, the range of the Alburni is definitely a complex 2D structure, as confirmed by the multiplicity of amplification bands apparent from the simulated data, dominated by a broad peak between 0.8 s and 2 s and a secondary peak at ~ 3-4 s. Following Cauzzi et al. (2010), the long-period amplification is relatively well explained by the fundamental vibration period of the uniform fixed-free shear-beam, with δ_l = 1500 - 300 = 1200 m, β = 1200 ms^{-1}, and therefore T_0 = 4 s. The first and second higher modes of the same shear-beam would occur at ~ 1.3 s and 0.8 s, respectively, very close to the largest amplification peak of Fig. 2.3 (rhs). This partially confirms the preliminary results of Cauzzi et al. (cit.) who, for thickset 2D features like the Mt. Morrone bordering the Sulmona (Central Italy) basin, found the maximum topographic amplification in the frequency bands representative of the higher models of the mountain as an idealised shear-beam. Note that for simple 2D structures, Cauzzi et al. (cit.) confirmed the vibration periods suggested by Paolucci (2002) and observed that, in many cases (obviously depending on the ratio δ_l/W), they tend to be close to fundamental modes of the reliefs modelled as idealised shear-beams.

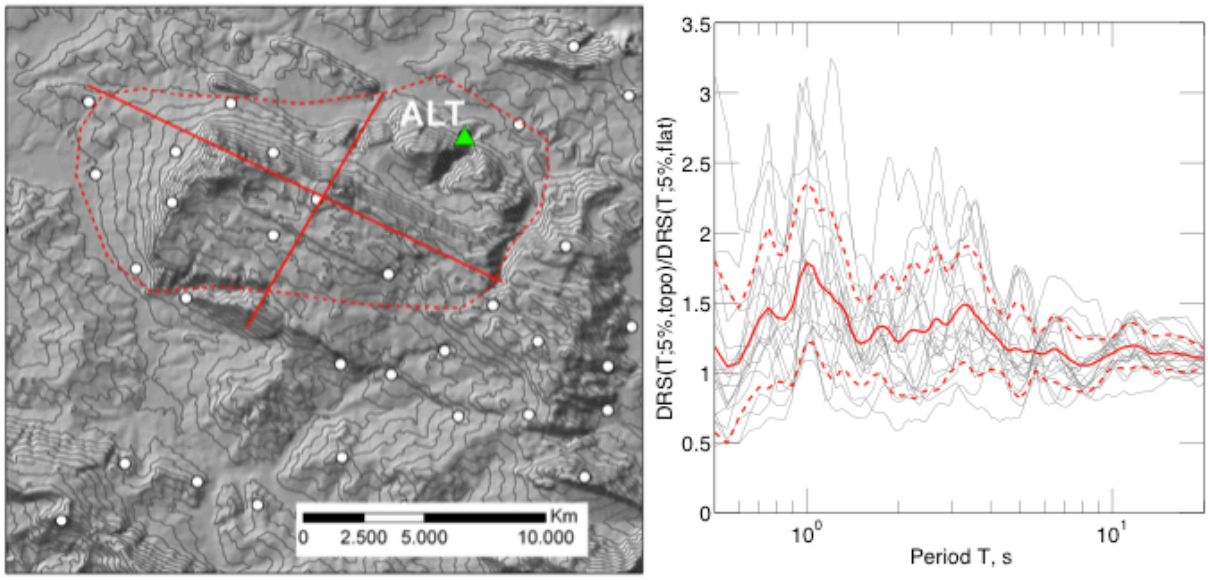

Figure 2.3. (lhs) Digital elevation model (DEM) of the area of the Alburni mountain range. Note the strong-motion station ALT (green triangle), the receivers of the numerical model (white circles) and the geometrical characteristics of the relief: the base of the mountain (dashed red curve) and the trace of two representative cross-sections (red solid lines); (rhs) Topographic amplification at the receivers located within the base area of the mountain, all data (grey curves), mean and standard deviation (red curves).

2.2.3. Amplification at 3D topographic irregularities

A simple and representative example of 3D structure is the hills of the city of Potenza, shown in Fig. 2.4, with maximum elevation of 1280 m a.s.l.. The spectral amplification as obtained from the spectral ratios computed from the synthetic waveforms is broadband and characterised by a multiplicity of maxima between 0.8 s and 6 s, dominated by a peak between 1 s and 3 s. The vibration periods

corresponding to the largest amplification peak can be partially explained by means of the theory of vibration of the shear-beam with δ_l = 1280 - 230 = 1050 m, β = 1200 ms^{-1}, and therefore T_0 = 3.5 s, at the upper bound of the observed amplification range. The first higher model of the same shear-beam would be at ~ 1.2 s, very close to the largest peak in Fig. 2.4(rhs). As for the case described in section 2.2.2, these results confirm the preliminary findings of Cauzzi et al. (2010) who, for 3D structures, found the dominant periods of topographic amplification to be roughly bounded by the fundamental and first higher mode of the shear-beam, with amplification levels generally lower than those observed for the 2D cases.

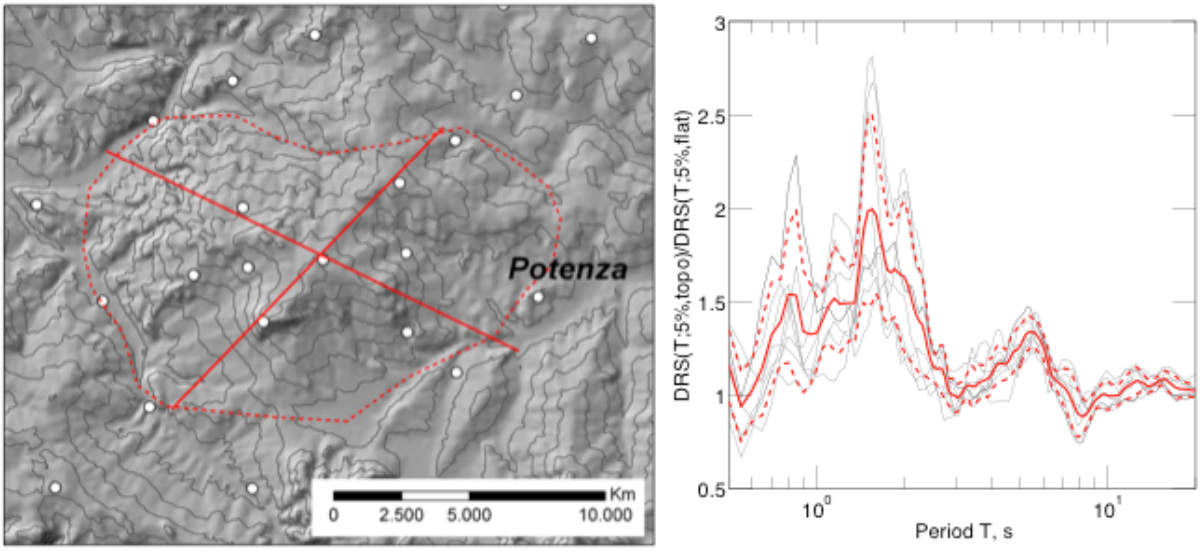

Figure 2.4. Same as Fig. 2.3, for the area around the city of Potenza.

3. TOPOGRAPHIC AMPLIFICATION FROM REAL DATA

The aim of this section is to critically compare the results obtained on synthetic data with a set of real cases provided by weak- and strong-motion recording at stations with pronounced topography in Italy and Switzerland. The dataset available for the analyses is briefly presented in Section 3.1, while representative results are summarised in Section 3.2.

3.1. Assembling a test dataset for topographic amplification studies

The simple criteria adopted in this study to assemble the dataset were: a) rock sites on topography class T3 or T4 of the Italian Building Code (NTC, 2008 – see Tab. 1.1); b) availability of at least 2 eq. recordings with magnitude M_W > 4 within 150 km distance; c) station pertaining to the Italian strong-motion network (RAN) or to the Swiss digital networks (strong-motion and broadband). The geomorphological classification of the stations was performed *via* GIS. The assembled dataset includes 7 stations, as listed in Tab 3.1.

Table 3.1. Italian and Swiss stations in the assembled dataset.

Station code	*Nation*	*# of selected eq. recordings*	*Magnitude (min-max); Distance (min-max)*	*Topography class (NTC, 2008)*
AQP	Italy	7	4.1 – 5.6; 1 – 15 km	T3
ASS	Italy	27	4 – 6.3; 15 – 113 km	T3
CSC	Italy	2	5.6 – 5.8; 9.3 – 22 km	T3
MMP	Italy	6	5.1 – 6.3; 49 – 59 km	T3
MTR	Italy	10	4.1 – 6.3; 9 – 33 km	T3
SMP	Italy	2	4.9 – 5.4; 60 – 61 km	T3
HASLI	Switzerland	2	4 – 4.4; 125 -103 km	T4

The source of the recordings of the Italian strong-motion network was the Italian Accelerometric Archive (ITACA, http://itaca.mi.ingv.it), while Swiss records were accessed using the webinterface available at http://arclink.ethz.ch.

3.2. Results

Due to the obvious lack of reference rock stations with flat topography for each site, elastic 5%-damped response spectra were computed over a broad period range from the selected ground motions and compared with two consolidated ground motion prediction equations (GMPEs), namely: Cauzzi and Faccioli (2008), CF08, global model dominated by Japanese strong-motion data; and Bindi et al. (2010), BEA10, specifically derived for application in Italy based on the Italian Accelerometric Archive. The CF08 model is amongst the global GMPEs selected within the European project SHARE for contributing to the logic tree for shallow active crustal regions (Delavaud et al., 2012). In spite of the moment magnitude range (5-7.2) of the calibration dataset of CF08, the prediction model has recently proved to adequately predict the spectra of recordings from low energy events, with magnitudes as low as 3.8 (Beauval et al., 2012). Residuals with respect to each ground motion prediction model where computed at each station j for each earthquake recording k based on the observed and predicted spectra as follows:

$$r_{jk}(T;GMPE,5\%) = \log_{10}\left(\frac{observed\_spectrum_{jk}(T;5\%)}{predicted\_spectrum_{jk}(T;GMPE,5\%)}\right) \quad (3.1)$$

Subsequently the mean and the standard error of the residuals at each station were computed and plotted as a function of vibration period T. Figg. 3.1, 3.2 and 3.3 show that the vibration period range where maximum residuals are found is independent on the GMPE adopted as a reference. Considering the totally different reference datasets of the adopted GMPEs, their different definition of the response variable, functional form and representation of site effects, this should be considered as a remarkable result, suggesting that the amplification effects observed on the residuals are related to specific response characteristics at the stations. Relating these amplifications to the topographic features at the recording sites is the subject of the present subsection.

A first interesting case amongst those considered in this study is represented by the Italian station ASS (Assisi, Fig. 3.1), located in Central Italy, with a large number of recordings of the Umbria-Marche earthquake sequence occurred between 1997 and 1998. Amplification w.r.t. both GMPEs is apparent between 0.2 s and 0.6 s. The station is located at the WWN edge of a 3D relief featuring two 2D appendixes pointing NNE and WWN. If the 3D relief as a whole is considered (see Fig. 3.1), the fundamental mode of the idealised shear-beam with δ_1 = 190 m occurs at ~ 0.6 s and the first higher mode at ~ 0.2 s, considering a representative average value of β = 1200 ms^{-1}. If only the 2D appendix where the station is located is considered, then the approach of Paolucci (2002) leads to estimate $T_{0\text{-}SH}$ ~ 0.7 s and $T_{0\text{-}SV}$ ~ 0.5 s. That is, both approaches can satisfactorily explain the apparent amplification phenomena at station ASS, provided a geophysical misclassification of the recording site can be definitely excluded.

Another interesting case from Central Italy is given by station CSC (Cascia), located at the foot of the NE edge of a complex 2D relief, with variable cross section (see Fig. 3.2), where amplification w.r.t. the GMPEs is observed over a broad period range between 0.1 s and 2 s, with a dominant peak between 0.4 s and 0.8 s. If the relief as a whole is considered (see Fig. 3.2), the fundamental mode of the idealised shear-beam with δ_1 = 295 m and β = 1200 ms^{-1} occurs at ~ 0.9 s and the first higher mode at ~ 0.3 s, respectively at the upper and lower bound of the observed amplification period range. If only the 2D appendix where the station is located is considered, then the approach of Paolucci (cit.) gives $T_{0\text{-}SH}$ ~ 0.38 s and $T_{0\text{-}SV}$ ~ 0.53 s, very close to the periods corresponding to peak amplification in the residuals. Therefore, also in this case, both approaches can satisfactorily explain the apparent amplification phenomena at station CSC.

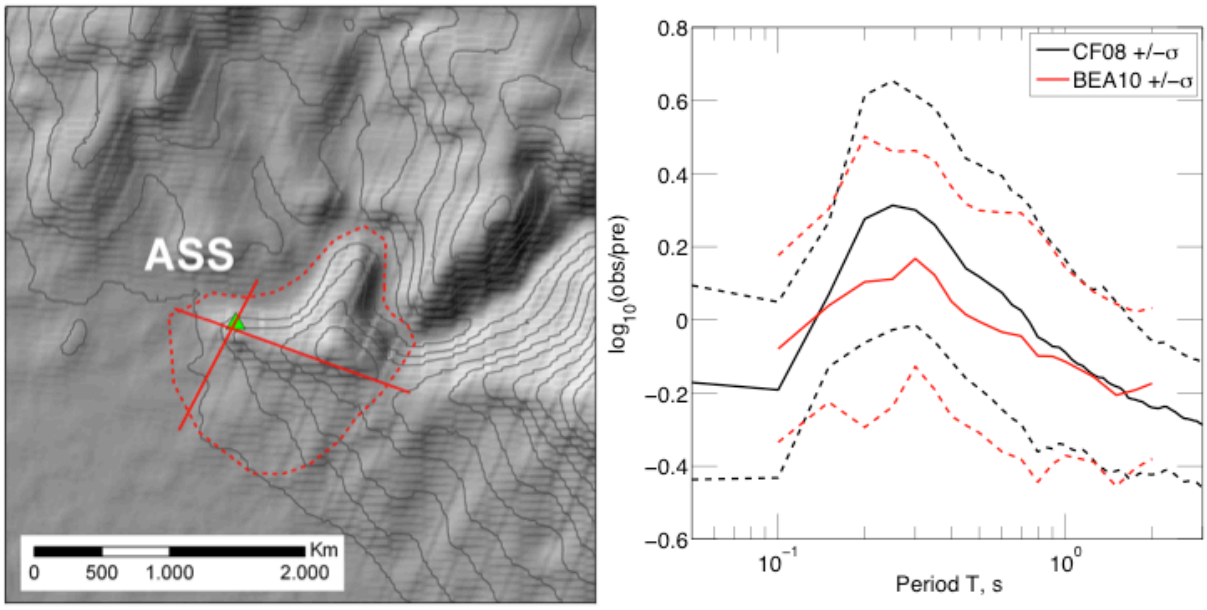

Figure 3.1. (lhs) Digital elevation model (DEM) of the area around the Italian station ASS (Assisi), indicated by the green triangle; (rhs) Topographic amplification at station ASS obtained from earthquake recordings, as described in the text.

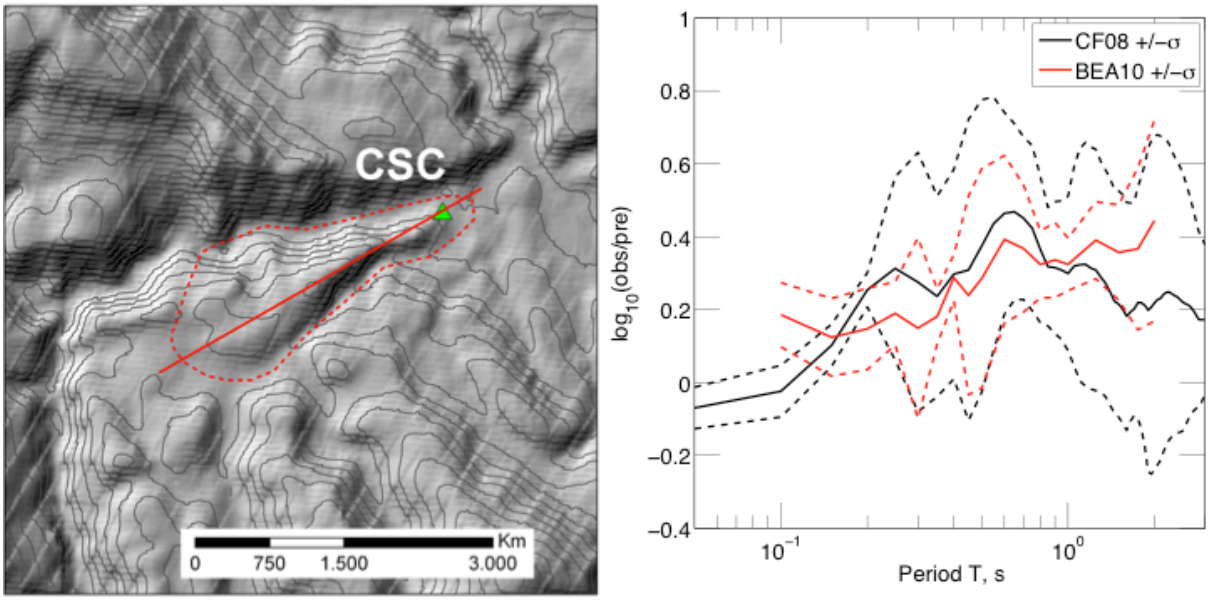

Figure 3.2. Same as Fig. 3.1, for stations CSC (Cascia).

As additional study case from Switzerland, amplification at station HASLI (Hasliberg) is depicted in Fig. 3.3 (rhs). Located on top of a ridge, the station is characterised by a complex topographic irregularity, bounded to the South and to the East by steep slopes. The residuals w.r.t. the selected GMPEs seem to suggest the largest amplification phenomena to occur in the period range 0.5 – 1 s. Based on the geometry of the ridge (maximum width ~ 1800 m, δ_l ~ 1000 m), this amplification effect can be explained following Paolucci (cit.) and Cauzzi et al. (cit.), if average β ~ 2000 ms^{-1} is assumed for the relief, some 25% higher than the shear-wave velocity at the recording site.

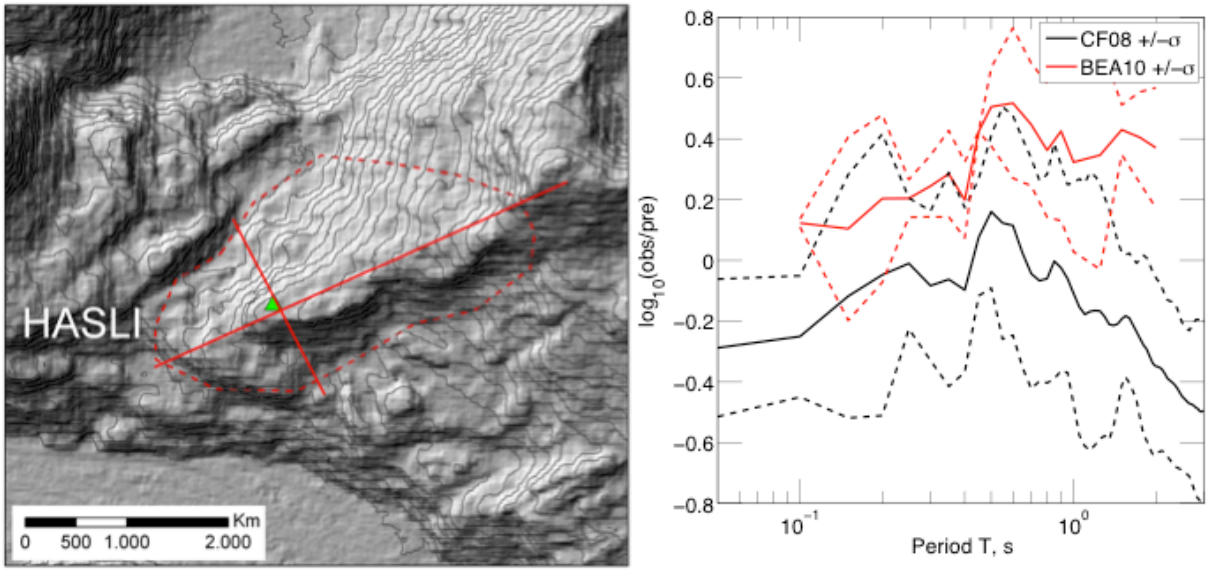

Figure 3.3. Same as Fig. 3.1, for the Swiss station HASLI (Hasliberg).

4. DISCUSSION AND CONCLUSIONS, A ROADMAP FOR IMPLEMENTATION IN GMPES

In this contribution, use has been made of 3D spectral element models and real earthquake recordings in Italy and Switzerland to complement and discuss the preliminary findings of Cauzzi et al. (2010). These authors, starting from the work of Paolucci (2002), proposed a more general reference framework to introduce topographic amplification factors in GMPEs or seismic hazard evaluations, as a function of the geometry of the relief and of its average mechanical properties. In spite of the relatively successful confirmations obtained in the present study, the real data examples presented herein reveal the challenges and the practical issues of the proposed approach, the definition of the geometry of the relief being prone to a certain level of subjectiveness or, better, of expert judgement. Additionally, studies concerning possible wrong geotechnical/geophysical characterisation at the recording sites should be conducted, especially for those regions where seismic stations are still classified on the basis of geological maps without detailed site investigations. Indeed, the practical application of the results of this study would require as a first step the preparation of guidelines for the classification of topographic irregularities, based on the results of numerical simulations, where the factors controlling the ground motions at specific site can be clearly identified and understood, and the difficulty posed by paucity of available real earthquake data could be easily overlooked. Based on the aforementioned guidelines, GMPEs developers would then need to inspect their datasets with the aim of classifying all stations on irregular topography (the simple selection adopted for practical reasons in this study is not representative of all possible real cases) and segregate them into different classes (by dummy variables), such as: i) simple 2D configurations (where the dominant periods of topographic amplifications are expected to be those suggested by Paolucci, cit.) and ii) complex 2D configurations / 3D configurations (where the dominant periods are apparently related to the fundamental mode and higher models of the relief described as an idealised shear-beam and expected amplitudes are generally lower than in the 2D cases). The amplification within each class could then be modelled as a simple function of the normalised height H (see Eqn. 1.2) and the ratio δ_l/W, that implicitely takes into account the average slope values of the relief at hand. Future work in this sense will be carried out based on the Japanese strong-motion dataset.

AKCNOWLEDGEMENT

We are thankful to Roberto Paolucci and Antonio Rovelli for their encouraging the development of this study, their careful revision of the manuscript and critical discussion of the results, which helped us in significantly improving the quality of this contribution.

REFERENCES

Ameri G., Emolo A., Pacor F. and Gallovič, F. (2011). Ground-Motion Simulations for the 1980 M 6.9 Irpinia Earthquake (Southern Italy) and Scenario Events. *Bull. Seism. Soc. Am.* **101:3**, 1136-1151.

Bindi, D., Luzi, L., Massa, M. and Pacor, F. (2011). Horizontal and vertical ground motion prediction equations derived from the Italian Accelerometric Archive (ITACA). *Bull. Earthq. Eng.* **8:5**, 1209-1230.

Bindi, D., Luzi, L., Pacor, F. and Paolucci, R. (2012). Identification of accelerometric stations in ITACA with distinctive features in their seismic response. Bull. Earthq. Eng. **9:6**, 1921-1939.

Beauval, C., Tasan, H., Laurendau, A., Delavaud, E., Cotton, F., Guéguen, P. and Kuehn, N. (2012). On the testing of ground motion prediction equations against small magnitude data. *Bull. Seism. Soc. Am.*, in press.

Blevins, R.D. (1979). Formulas for natural frequency and mode shape, Van Nostrand Reinhold, New York.

Cauzzi, C. and Faccioli, E. (2008). Broadband (0.05 to 20 s) prediction of displacement response spectra based on worldwide digital records. *J. Seismol.* **12**: 453-475.

Cauzzi , C., Faccioli, E., Stupazzini, M. and Villani, M. (2010). Including topographic amplification factors in GMPEs by means of 3D simulations of ground motions. *14th European Conference of Earthquake Engineering*. Paper no. 1382.

Comité Européen de Normalisation, CEN (2004). Eurocode 8: Design of structures for earthquake resistance Part 1: General rules, seismic actions and rules for buildings, Brussels.

Cultrera G., Cirella A., Spagnuolo E., Herrero A., Tinti E. and Pacor, F. (2010). Variability of kinematic source parameters and its implication on the choice of the design scenario. *Bull. Seism. Soc. Am.* **100:3**, 941-953.

Delavaud, E., Cotton, F., Akkar, S., Scherbaum, F., et al. (2012). Toward a ground motion logic tree for probabilistic seismic hazard assessment in Europe. *J. Seismol.*, in press.

Faccioli, E., Maggio, F., Paolucci, R. and Quarteroni, A. (1997). 2D and 3D elastic wave propagation by a pseudo-spectral domain decomposition method. *J. Seismol.* **1**, 237-251.

Faccioli, E., Vanini, M. and Frassine, L. (2002) "Complex" site effects in earthquake ground motion, including topography. *12th European Conference on Earthquake Engineering.* Paper no. 844.

Massa, M., Lovati, S., D'Alema, E., Ferretti, G. and Bakavoli, M. (2010). An experimental approach for estimating seismic amplification effects at the top of a ridge, and the implication for ground-motion predictions: the case of Narni. Central Italy. *Bull. Seism. Soc. Am.* **100:6**, 286-301.

Norme Tecniche per le Costruzioni, NTC (2008). DM 140108, Ministero delle Infrastrutture, Gazzetta Ufficiale Roma.

Paolucci, R. (2002). Amplification of earthquake ground motion by steep topographic irregularities. *Earthq. Eng. Struct. Dyn.* **31**, 1831-1853.

Stupazzini, M., Paolucci, R. and Igel, H. (2009). Near-Fault Earthquake Ground-Motion Simulation in the Grenoble Valley by a High-Performance Spectral Element Code. *Bull. Seism. Soc. Am.* **99**, 286-301.